



# Two aspartic proteases, BnaAP36s and BnaAP39s, regulate pollen tube guidance in *Brassica napus*

Lulin Wang · Xiaomei Liang · Shengwei Dou ·  
Bin Yi · Tingdong Fu · Chaozhi Ma · Cheng Dai

Received: 31 October 2022 / Accepted: 31 March 2023 / Published online: 5 April 2023  
© The Author(s), under exclusive licence to Springer Nature B.V. 2023

**Summary** Pollen tube (PT) growth towards the micropyle is critical for successful double fertilization. However, the mechanism of micropyle-directed PT growth is still unclear in *Brassica napus*. In this study, two aspartate proteases, BnaAP36s and BnaAP39s, were identified in *B. napus*. BnaAP36s and BnaAP39s were localized to the plasma membrane. The homologues of *BnaAP36* and *BnaAP39* were highly expressed in flower organs, especially in the anther. Sextuple and double mutants of *BnaAP36s* and *BnaAP39s* were then generated using CRISPR/Cas9 technology. Compared to WT, the seed-set of *cr-bnaap36* and *cr-bnaap39* mutants was reduced by 50% and 60%, respectively. The reduction in seed-set was also found when *cr-bnaap36* and *cr-bnaap39* were used as the female parent in a reciprocal cross assay. Like WT, *cr-bnaap36* and *cr-bnaap39* pollen were able to germinate and the relative PTs were able to elongate in style. Approximately 36% and 33% of *cr-bnaap36* and *cr-bnaap39* PTs, respectively, failed to grow towards the micropyle, indicating that

BnaAP36s and BnaAP39s are essential for micropyle-directed PT growth. Furthermore, Alexander's staining showed that 10% of *cr-bnaap39* pollen grains were aborted, but not *cr-bnaap36*, suggesting that *BnaAP39s* may also affect microspore development. These results suggest that BnaAP36s and BnaAP39s play a critical role in the growth of micropyle-directed PTs in *B. napus*.

**Keywords** *Brassica napus* · *BnaAP36s* · *BnaAP39s* · CRISPR/Cas9 · Pollen tube guidance · Seed-set

## Introduction

In angiosperms, successful double fertilization plays a crucial role in plant reproduction. Mature pollen grains land on the stigma, and the compatible interaction between pollen and papilla cells triggers pollen hydration and germination (Palanivelu and Tsukamoto 2012). The germinated pollen tubes (PTs) grow towards the ovule, guided by internal signals, and then deliver two sperm cells into the embryo sac, which fuse with the egg and central cells to complete double fertilization (Swanson et al. 2004; Dresselhaus et al. 2016; Berger et al. 2008). Unlike animal sperm, plant sperm cannot move autonomously and rely on the transport of PTs to successfully reach the ovule. Therefore, the growth and guidance of PTs is key to complete double fertilization (Weterings and Russell

**Supplementary Information** The online version contains supplementary material available at <https://doi.org/10.1007/s11032-023-01377-1>.

L. Wang · X. Liang · S. Dou · B. Yi · T. Fu · C. Ma · C. Dai  
National Key Laboratory of Crop Genetic Improvement,  
Huazhong Agricultural University, Wuhan 430070, China

L. Wang · X. Liang · S. Dou · C. Ma · C. Dai (✉)  
Hubei Hongshan Laboratory, Wuhan 430070, China  
e-mail: cdai@mail.hzau.edu.cn

2004; Márton et al. 2005; Zhong and Qu 2019), which is controlled by a complex signaling cascade involving male and female gametes (Lausser and Dresselhaus 2010; Higashiyama and Takeuchi 2015).

Plant male and female gametes secrete a variety of signaling substances to regulate the growth and guidance of pollen grains. In Arabidopsis, the small peptide LURE1.2 secreted by the ovule is recognized by the pollen-specific receptor-like kinase 6 (PRK6), and directs the ovule to specifically attract its own pollen tubes, thereby promoting interspecies reproductive isolation (Zhong et al. 2019; Zhang et al. 2017b; Wang et al. 2016). The absence of receptor-like kinases in Arabidopsis, such as Feronia (FER), ANJEA (ANJ), and HERCULES RECEPTOR KINASE 1 (HERK1), results in the unrestricted elongation of PTs, even entering the micropylar and reaching the synergid cells (Escobar-Restrepo et al. 2007; Galindo-Trigo et al. 2020). Further studies indicate that the rapid alkalization factor (RALF) peptides expressed by PTs are the ligands of FER, ANJ and HERK1 (Zhong et al. 2022). Mutation of these peptides results in the simultaneous emergence of multiple pollen tubes from the septum (Zhong et al. 2022). After fertilization, EGG CELL-SPECIFIC1 (ECS1 and ECS2) are secreted by the egg cells and degrade LURE1, preventing multiple sperm from entering the egg cell (Yu et al. 2021). In maize, down-regulation of the polypeptide ZmEA1 gene results in egg sterility, suggesting that ZmEA1 is involved in the signaling process of PTs attraction in maize (Márton et al. 2005). However, the mechanism of PTs growth and guidance is very complex and many regulatory pathways remain to be discovered.

Aspartate proteases (APs) are a class of important proteolytic enzymes that contain two Asp residues within the conserved Asp-Thr/Ser-Gly motifs at the active site (Simões and Faro 2004; Takahashi et al. 2008). The APs are activated under acidic pH condition, and the activates of APs are specifically inhibited by pepstatin A (Simões and Faro 2004; Takahashi et al. 2008). APs exist widely in many plants and play an indispensable role in plant development, stress responses, and gamete formation. For instance, tobacco CND41 is a DNA-binding aspartic protease localized in the chloroplast (Takahashi et al. 2008). Overexpression of CND41 in tobacco promotes leaf senescence, suggesting that CND41 plays an important role in leaf senescence (Takahashi et al. 2008; Kato et al. 2005). An atypical aspartic protease (ASPR1) modulates

lateral root development in Arabidopsis (Soares et al. 2019). Overexpression of aspartate protease constitutive disease resistance (*CDR1*) in Arabidopsis and rice can enhance salicylic acid-mediated disease resistance (Xia et al. 2004; Prasad et al. 2009). The Arabidopsis *AtASPG1* (ASPARTIC PROTEASE IN GUARD CELL 1) positively regulates ABA-mediated drought resistance (Yao et al. 2012). Subsequent studies suggest that *AtASPG1* is also involved in the GA signaling-mediated storage protein degradation (Shen et al. 2018). Moreover, rice aspartate proteases, OsAP25, OsAP37 and OsAP65, are essential for tapetum degradation and pollen tube formation during pollen grain development (Huang et al. 2013; Niu et al. 2013). The Arabidopsis aspartic proteases encoding genes, *AtA36* and *AtA39*, are highly expressed in pollen and pollen tubes (Gao et al. 2017b). Knocking-out of *AtA36* and *AtA39* leads to programmed apoptosis of microspores, degeneration of female gametophytes, and impaired pollen tube guidance (Gao et al. 2017b). These findings suggest functional specialization of plant APs and tight regulation of AP activity in different biological processes.

*Brassica napus* is an important oilseed crop derived from spontaneous hybridization between *Brassica rapa* and *Brassica oleracea* (Hu et al. 2022; Chen et al. 2023). We have previously identified 154 APs genes in *B. napus* (Huang et al. 2022). Here, two plasma membrane localized aspartate proteases, *BnaAP36s* and *BnaAP39s*, were identified in *B. napus*. The homologs of *BnaAP36* and *BnaAP39* were mainly expressed in flower organs, especially in the anther. The sextuple and double mutants of *BnaAP36* and *BnaAP39* were then generated by CRISPR/Cas9 genome editing technology. The sextuple and double mutants of *BnaAP36* and *BnaAP39* displayed lower seed-set, and PTs failed to grow towards the micropyle. Our results indicate that *BnaAP36s* and *BnaAP39s* are the first APs with an expected role in the regulation of PTs-guided growth in *B. napus*, which will elucidate the fundamental role of APs in pollen grain survival and egg-sperm communication in plants.

## Results

*BnaAP36s* and *BnaAP39s* are highly expressed in flower organs in *B. napus*

We previously identified 154 APs genes in *B. napus* (Huang et al. 2022). Among them, *BnaAP36* and

*BnaAP39* homologs were significantly up-regulated after pollination (Fig. 1A and B). There were six and two homologs of *BnaAP36* and *BnaAP39* in *B. napus*, respectively (Table S1). Based on the chromosome localization, we named these *BnaAP36* and *BnaAP39* homologs as *BnaA08.AP36*, *BnaC08.AP36*, *BnaA04.AP36*, *BnaC04.AP36*, *BnaA05.AP36*, *BnaC06.AP36*, *BnaA06.AP39* and *BnaC03.AP39*, respectively (Fig. S1, Table S1). The protein sequences of *BnaAP36s* and *BnaAP39s* shared high identity with Arabidopsis AP36 and AP39 homologs, ranging from 81.19% to 85.59%, and 83.01% to 83.05%, respectively (Fig. S2 and S3). Domain analysis revealed that both *BnaAP36s* and *BnaAP39s* contain signal peptide in N-terminal, and aspartic protease domain in C terminal (Fig. S2 and S3). Like other eukaryotic aspartic proteases, both *BnaAP36s* and *BnaAP39s* contain two catalytic Asp residues within two conserved active sites with the sequence Asp-Thr/Ser-Gly-Ser/Thr (Fig. S2 and S3), suggesting that these proteins could be functional as aspartate proteases.

Subsequently, the tissue expression data of *BnaAP36s* and *BnaAP39s* were obtained from BnTIR (<http://yanglab.hzau.edu.cn/BnTIR>) (Liu et al. 2021). Six *BnaAP36* homologs were found to be highly expressed in 4 mm flower bud (Fig. S4 A-F). In particular, *BnaA08.AP36*, *BnaC08.AP36*, *BnaA04.AP36* and *BnaC04.AP36* were highly expressed in the anther (Fig. S4A-D). Compared to *BnaAP36s*, *BnaA06.AP39* and *BnaC03.AP39* were expressed in anther and 4 mm flower bud (Fig. S4G-H). To verify the RNA-seq results, the vegetative tissues (root, stem, leaf), flower buds (2 mm, 4 mm and 6 mm), open flower (sepal, petal, stigma, ovary, anther and filament), seed, and silique were collected, and the tissue expression pattern of *BnaAP36* and *BnaAP39* homologs was examined by RT-qPCR. In general, *BnaAP36s* and *BnaAP39s* were mainly expressed in flower buds, and less expressed in vegetative tissues (Fig. 1C and D). However, the expression of six *BnaAP36* homologues was quite different. For example, *BnaA08.AP36*, *BnaC08.AP36*, *BnaC04.AP36* and *BnaC06.AP36* were highly expressed in 6 mm flower buds; *BnaA04.AP36* was highly expressed in 4 mm and 6 mm flower buds; only *BnaA05.AP36* was highly expressed in 2 mm flower buds (Fig. 1C). The expression of two *BnaAP39s* gradually increased with the anther development (Fig. 1D). In open flowers, all the homologs of *BnaAP36* and *BnaAP39* showed the highest expression in the anther (Fig. 1E and F). In addition,

*BnaC08.AP36* and *BnaA06.AP39* were randomly selected to obtain the exact tissue expression pattern. Two *GUS* reporter constructs (*pBnaC08.AP36::GUS* and *pBnaA06.AP39::GUS*) were generated and individually transformed into Arabidopsis. The positive transgenic lines were obtained in T<sub>1</sub> generation and GUS staining assay was performed. The results showed that no significant GUS signal was observed in vegetative tissues in *pBnaC08.AP36::GUS* and *pBnaA06.AP39::GUS* Arabidopsis transgenic lines (Fig. 1G (i) and H (i)). The strong GUS signal was found in floral organs, such as sepal (Fig. 1G (ii, iii) and H (ii, iii)), stigma (Fig. 1H (iv)), ovary (Fig. 1G (iv) and H (iv)), anther and filament (Fig. 1G (v) and H (v)) in Arabidopsis transgenic lines.

Sequence analysis revealed that *BnaAP36s* and *BnaAP39s* were GPI-anchored proteins ([http://mendel.imp.ac.at/gpi/gpi\\_server.html](http://mendel.imp.ac.at/gpi/gpi_server.html)) (Fig. S5). To determine the subcellular localization of *BnaAP36s* and *BnaAP39s*, we transiently expressed the *BnaC08.AP36-GFP* and *BnaA06.AP39-GFP* fusion genes in tobacco epidermal cells. The fusion proteins were predominantly localized to the plasma membrane (PM) (Fig. 1I and J), which was colocalized with the PM marker CBL-RFP (Yang et al. 2021). These results indicate that *BnaAP36s* and *BnaAP39s* belong to the membrane-anchored aspartic proteases.

Generation the functionally deficient mutants of *BnaAP36s* and *BnaAP39s* in *B. napus*

To study the function of *BnaAP36s* and *BnaAP39s* in *B. napus*, we then generated mutant lines of *BnaAP36s* and *BnaAP39s* using the CRISPR/Cas9-mediated genome editing toolbox (Tang et al. 2018). Four single-guide RNAs (sgRNAs) were designed to target the homologous of *BnaAP36* (Fig. 2A). Among them, sgRNA1 targeted the first exon of *BnaA08.AP36*, *BnaC08.AP36*, *BnaA05.AP36* and *BnaC06.AP36*; sgRNA2 targeted the first exon of *BnaA05.AP36* and *BnaC06.AP36*; sgRNA3 targeted the sixth exon of *BnaA08.AP36*, *BnaC08.AP36*, *BnaA04.AP36*, *BnaC04.AP36*, and *BnaA05.AP36*; and sgRNA4 targeted the seventh exon of all six *BnaAP36s* (Fig. 2A). Two sgRNAs, sgRNA5 and sgRNA6, were designed to target the first and second exons of the two *BnaAP39s*, respectively (Fig. 2C). These two constructs were then individually transformed into *B. napus* WT (Westar, self-compatible).

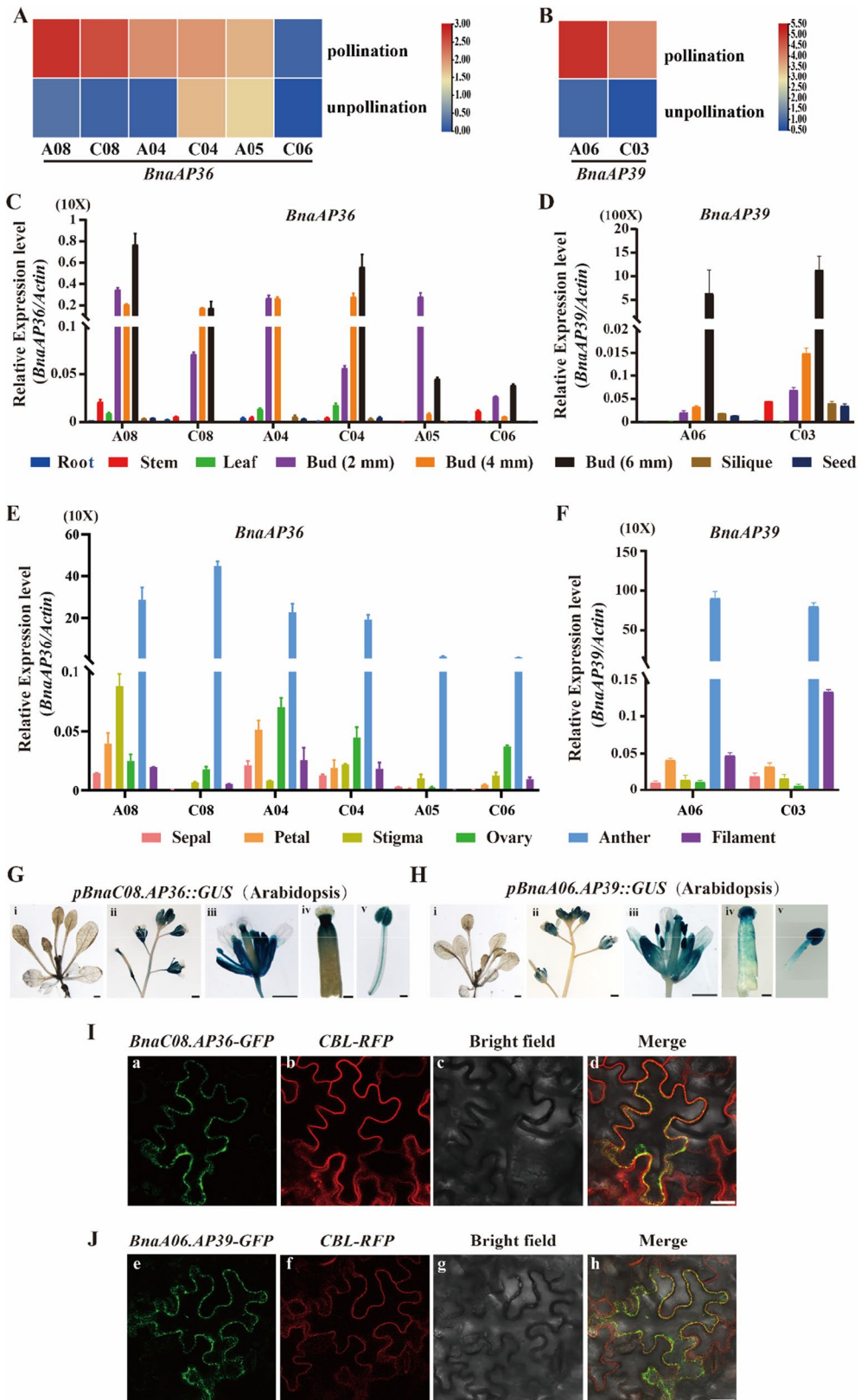




**Fig. 1** Expression patterns of *BnaAP36s* and *BnaAP39s* genes in *B. napus*. (A) and (B) Expression of homologues of *BnaAP36s* (A) and *BnaAP39s* (B) in stigmas before and after pollination. The data was obtained from our previous study (Zhang et al. 2017a) (C) and (D) The bar graphs showed the relative expression levels of *BnaAP36s* (C) and *BnaAP39s* (D) in vegetative tissues (root, stem, leaf), flower buds (2 mm 4 mm and 6 mm), seed, and silique. (E) and (F) The bar graphs showed the relative expression levels of *BnaAP36s* (E) and *BnaAP39s* (F) in sepal, petal, stigma, ovary, anther, and filament. (G) and (H) Images showing the GUS staining of *BnaC08.AP36pro::GUS* Arabidopsis transgenic lines (G) and *BnaA06.AP39pro::GUS* Arabidopsis transgenic lines (H). (I) and (J) The images showed the subcellular localization of *BnaC08.AP36* (I) and *BnaA06.AP39* (J) after transient expressed in *N. benthamiana* epidermal cells. The CBL-RFP protein was used as membrane marker. Scale bar=50  $\mu$ m. In (C) to (F), values were the mean  $\pm$  SE of three biological replicates. *BnaActin7* acts an internal control. The expression level of each gene was calculated using the  $2^{-\Delta\Delta CT}$  method. In (G) and (H), i: vegetative tissue; ii and iii: flower tissue; iv: pistil; v: stamens. i-iii: Scale bar = 1 mm, iv-v: Scale bar = 0.1 mm

Ten and nine mutants of *BnaAP36s* and *BnaAP39s*, respectively, were isolated in T<sub>0</sub> generation (Tables 1 and 2). Short deletions or insertions at sgRNA target sites were validated by Hi-TOM sequencing (Fig. 2, Tables 1 and 2). The editing efficiency of the sgRNAs was quite variable. For example, no mutation was identified at the target sites of sgRNA1, sgRNA2 and sgRNA3, whereas sgRNA4 simultaneously generated mutations at six *BnaAP36s* (Fig. 2B, Table 1). In the T<sub>0</sub> generation, *cr-bnaap36-3* and *cr-bnaap36-6* were homozygous sextuple mutants of *BnaAP36s*, while the other *cr-bnaap36* lines and all *cr-bnaap39* lines were heterozygous at different sgRNAs targeted sites (Tables 1 and 2). In the T<sub>1</sub> generation, the progeny of *cr-bnaap36* homozygous mutants (L3 and L6) were all homozygous at the sgRNA4 targeted site (Table S2), and the genotype of other sgRNA targeted sites was WT (sgRNA1, sgRNA2 and sgRNA3) (Table S2). The segregation ratio followed the Mendelian law (Table S2). At the sgRNA5 targeted site, the numbers of wild type : heterozygote : homozygote were 6: 14: 0 (*cr-bnaap39*, L4, *BnaA06.AP39*), 6: 14: 0 (*cr-bnaap39*, L4, *BnaC03.AP39*), 6: 2: 12 (*cr-bnaap39*, L9, *BnaA06.AP39*), and 6: 1:13 (*cr-bnaap39*, L9, *BnaC03.AP39*) (Table S3); while the numbers of wild type : heterozygote : homozygote were 11: 1: 8 (*cr-bnaap39*, L4, *BnaA06.AP39*), 9: 3: 8 (*cr-bnaap39*, L4, *BnaC03.AP39*), 20: 0: 0 (*cr-bnaap39*, L9, *BnaA06.AP39*), and 7: 0:

13 (*cr-bnaap39*, L4, *BnaC03.AP39*) (Table S3) at sgRNA6 targeted site. We speculate that the small number of populations were tested resulted in a segregation ratio of offspring that did not match the classical Mendelian segregation ratio of 1:2:1.

Disruption of *BnaAP36s* or *BnaAP39s* genes result in lower seed setting rate

Subsequently, the homozygotes of *cr-bnaap36* (sextuple mutant, L3 and L6) and *cr-bnaap39* (double mutant, L4 and L9) were isolated by Hi-TOM sequencing in the T<sub>1</sub> generation (Fig. 2B and D; Tables 1 and 2), and grown in the field for phenotype observation. Like WT (Westar) and transgenic negative plants (no editing), all mutants showed normal development during the vegetative stage, and the floral organs didn't show any defect in these mutant lines (data not shown). Then, the silique lengths of *cr-bnaap36* after self-crossing were approximately 3.8-4.9 cm, which was shorter than wild-type (WT) and transgenic negative plants (NC) after self-crossing (WT: 5.5 cm; NC: 5.6 cm) (Fig. 3A and B). Seed-set was also reduced in *cr-bnaap36* after self-crossing, approximately 11-18 seeds per silique in *cr-bnaap36*, which was significantly less than WT and transgenic negative plants after self-crossing (WT: 28 seeds per silique; NC: 27 seeds per silique) (Fig. 3C). To further investigate the role of male or female gametophytes in responsible for the seed-set reduction, the silique length and seed set were calculated using *cr-bnaap36* plants as the male or female parent in crosses with WT plants. When *cr-bnaap36* was used as the male parent, there was no difference in the silique length and the seed-set between *cr-bnaap36*  $\times$  wild-type and wild-type  $\times$  wild-type (Fig. 3A-C). When *cr-bnaap36* was used as the female parent, the silique length and the seed-set were reduced (silique length: 3.9-5.2 cm; and seed set: 12-19 seeds/ silique) (Fig. 3A-C), similar to the self-crossing of *cr-bnaap36*. Like *cr-bnaap36*, the silique lengths and the seed-set were also reduced in *cr-bnaap39* (Fig. 3D-F), and the seed-set reduction was observed after reciprocal crosses using *cr-bnaap39* as the female parent (Fig. 3D-F).

The viability of mature pollen grains in the *BnaAP36* and *BnaAP39* mutants was then examined by Alexander staining. No obvious differences

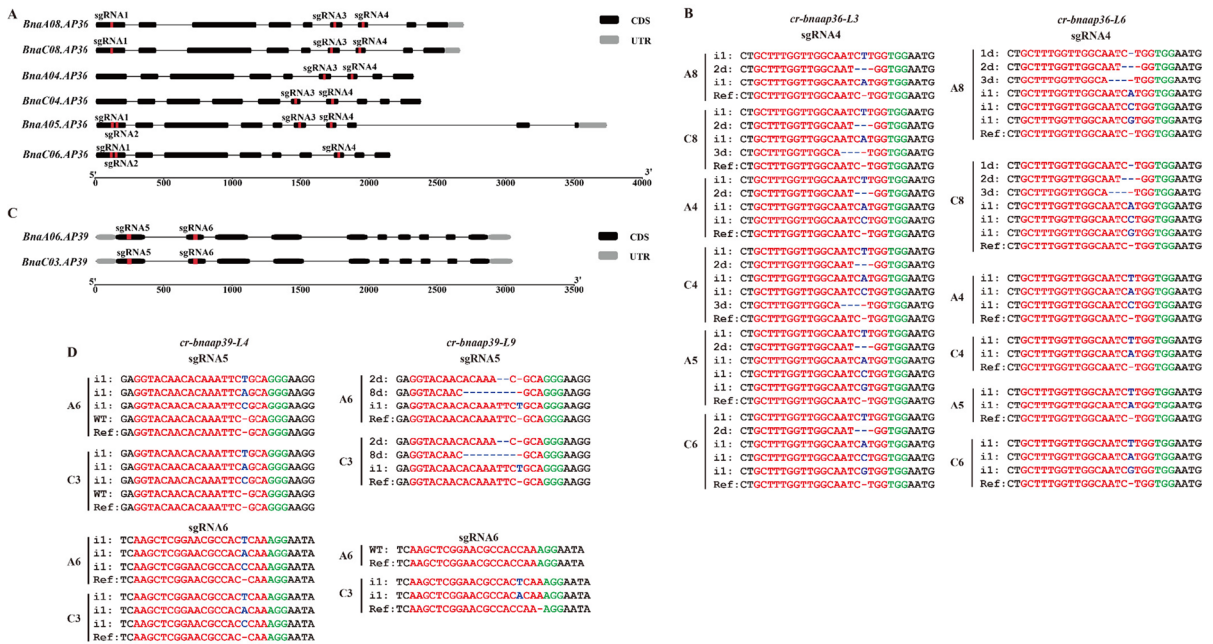


**Fig. 2** The genotypes of *B. napus* *BnaA36s* and *BnaAP39s* mutants. **(A)** The homologues of the *BnaAP36* gene model. Grey squares: UTR regions; black squares: exon regions; solid lines: introns; and small red squares: sgRNA target sites. **(B)** Genotype of the *cr-bnaap36* sextuple mutants. The protospacer adjacent motif (PAM) region was marked in green. The sgRNA was denoted in red. The mutation sites were indicated in blue. d#: # of bp deleted from target site; i#: # of bp inserted from target site; wt: wild type. **(C)** The homologues

of the *BnaAP39* gene model. Grey squares: UTR regions; black squares: exon regions; solid lines: introns; and small red squares: sgRNA targeted sites. **(D)** Genotype of the *cr-bnaap39* double mutants. The protospacer adjacent motif (PAM) region was marked in green. The sgRNA was denoted in red. The mutation sites were indicated in blue. d#: # of bp deleted from target site; i#: # of bp inserted from target site; wt: wild type

were observed in the mature pollen grains of the *cr-bnaap36* mutants compared to the WT (Fig. 4A and B). Approximately 9% of pollen grains of *cr-bnaap39-4* (8.4%) or *cr-bnaap39-9* (9.1%) mutants could not be stained by Alexander dye (Fig. 4A and B). These unstained pollen grains were smaller with abnormal cytoplasm (Fig. 4A). These results suggest that *BnaAP39* is essential for pollen grain viability.

**PTs in *BnaAP36s* and *BnaAP39s* mutants display abnormal micropylar guidance**

The very low ratio of inactive pollen in the *BnaAP36s* and *BnaAP39s* mutants could not explain why the lower seed-set was significantly higher than that of WT plants (Fig. 3). We therefore monitored pollen tube growth after self- and cross-pollination using the

aniline blue assay. The pollen grains of wild-type, *cr-bnaap36* (L3 and L6), *cr-bnaap39* (L4 and L9) germinated normally, and a large number of PTs could elongate and cross the stigma after 24 h (Fig. 5A and B), suggesting that the reduction in the seed-set isn't due to the failure of pollen - stigma recognition and PTs elongation.

We also followed the path of PTs growth towards the micropyles after self-pollination. Compared to the 88% that entered to the WT micropyles (Fig. 5C (i) and D), fewer PTs grew normally and directly entered the micropyles (*cr-bnaap36*: 64%-65%, *cr-bnaap39*: 66%-67%; Fig. 5D). Approximately 35%, and 33% of *cr-bnaap36* and *cr-bnaap39* pollen tubes showed abnormal guidance, and PTs grew on the ovule surface or twisting around the funicular surface, ultimately missing the micropyles (Fig. 5C (ii-iii) and D). The path of WT PTs was then followed after

**Table 1** Genotypic analysis of *BnaAP36s* mutants in T<sub>0</sub> and T<sub>1</sub> generations (The red labeled ID indicated the two individual lines in this study)

Plant ID	Generation	genotype at targets of <i>BnaA08.AP36</i>					genotype at targets of <i>BnaC08.AP36</i>					genotype at targets of <i>BnaA04.AP36</i>					
		sgRNA1	sgRNA2	sgRNA3	sgRNA4	sgRNA1	sgRNA2	sgRNA3	sgRNA4	sgRNA1	sgRNA2	sgRNA3	sgRNA4	sgRNA1	sgRNA2	sgRNA3	sgRNA4
<i>cr-bnaap36-L1</i>	T <sub>0</sub>	WT	WT	WT	Homo (id)	WT	WT	WT	Homo (id)	WT	WT	Homo (id)	WT	WT	WT	Homo (i)	
<i>cr-bnaap36-L2</i>	T <sub>0</sub>	WT	WT	WT	WT	WT	WT	WT	WT	WT	WT	WT	WT	WT	WT	WT	
<i>cr-bnaap36-L3</i>	T <sub>0</sub>	WT	WT	WT	Homo (id)	WT	WT	WT	Homo (id)	WT	WT	Homo (id)	WT	WT	WT	Homo (id)	
<i>cr-bnaap36-L3-1</i>	T <sub>1</sub>	WT	WT	WT	Homo (id)	WT	WT	WT	Homo (id)	WT	WT	Homo (id)	WT	WT	WT	Homo (id)	
<i>cr-bnaap36-L3-2</i>	T <sub>1</sub>	WT	WT	WT	Homo (id)	WT	WT	WT	Homo (id)	WT	WT	Homo (id)	WT	WT	WT	Homo (id)	
<i>cr-bnaap36-L3-3</i>	T <sub>1</sub>	WT	WT	WT	Homo (id)	WT	WT	WT	Homo (id)	WT	WT	Homo (id)	WT	WT	WT	Homo (id)	
<i>cr-bnaap36-L3-4</i>	T <sub>1</sub>	WT	WT	WT	Homo (id)	WT	WT	WT	Homo (id)	WT	WT	Homo (id)	WT	WT	WT	Homo (id)	
<i>cr-bnaap36-L3-5</i>	T <sub>1</sub>	WT	WT	WT	Homo (i)	WT	WT	WT	Homo (id)	WT	WT	Homo (id)	WT	WT	WT	Homo (id)	
<i>cr-bnaap36-L6</i>	T <sub>0</sub>	WT	WT	WT	Homo (id)	WT	WT	WT	Homo (id)	WT	WT	Homo (id)	WT	WT	WT	Homo (i)	
<i>cr-bnaap36-L6-1</i>	T <sub>1</sub>	WT	WT	WT	Homo (id)	WT	WT	WT	Homo (id)	WT	WT	Homo (id)	WT	WT	WT	Homo (i)	
<i>cr-bnaap36-L6-2</i>	T <sub>1</sub>	WT	WT	WT	Homo (id)	WT	WT	WT	Homo (id)	WT	WT	Homo (id)	WT	WT	WT	Homo (i)	
<i>cr-bnaap36-L6-3</i>	T <sub>1</sub>	WT	WT	WT	Homo (id)	WT	WT	WT	Homo (id)	WT	WT	Homo (id)	WT	WT	WT	Homo (i)	
<i>cr-bnaap36-L6-4</i>	T <sub>1</sub>	WT	WT	WT	Homo (id)	WT	WT	WT	Homo (id)	WT	WT	Homo (id)	WT	WT	WT	Homo (i)	
<i>cr-bnaap36-L6-5</i>	T <sub>1</sub>	WT	WT	WT	Homo (id)	WT	WT	WT	Homo (id)	WT	WT	Homo (id)	WT	WT	WT	Homo (i)	
<i>cr-bnaap36-L7</i>	T <sub>0</sub>	WT	WT	WT	Hetero	WT	WT	WT	WT	WT	WT	WT	WT	WT	WT	Hetero	
<i>cr-bnaap36-L8</i>	T <sub>0</sub>	WT	WT	WT	WT	WT	WT	WT	WT	WT	WT	WT	WT	WT	WT	WT	
<i>cr-bnaap36-L9</i>	T <sub>0</sub>	WT	WT	WT	WT	WT	WT	WT	WT	WT	WT	WT	WT	WT	WT	WT	
<i>cr-bnaap36-L10</i>	T <sub>0</sub>	WT	WT	WT	Homo (i)	WT	WT	WT	Homo (i)	WT	WT	Homo (i)	WT	WT	WT	Hetero	
<i>cr-bnaap36-L11</i>	T <sub>0</sub>	WT	WT	WT	Hetero	WT	WT	WT	Hetero	WT	WT	Hetero	WT	WT	WT	Hetero	
<i>cr-bnaap36-L12</i>	T <sub>0</sub>	WT	WT	WT	Hetero	WT	WT	WT	Hetero	WT	WT	Hetero	WT	WT	WT	Hetero	
Plant ID	Generation	genotype at targets of <i>BnaC04.AP36</i>					genotype at targets of <i>BnaA05.AP36</i>					genotype at targets of <i>BnaC06.AP36</i>					
<i>cr-bnaap36-L1</i>	T <sub>0</sub>	sgRNA1	sgRNA2	sgRNA3	sgRNA4	sgRNA1	sgRNA2	sgRNA3	sgRNA4	sgRNA1	sgRNA2	sgRNA3	sgRNA4	sgRNA1	sgRNA2	sgRNA3	sgRNA4
<i>cr-bnaap36-L2</i>	T <sub>0</sub>	WT	WT	WT	Homo (id)	WT	WT	WT	Homo (i)	WT	WT	Hetero	Homo (i)	WT	WT	WT	Homo (i)
<i>cr-bnaap36-L3</i>	T <sub>0</sub>	WT	WT	WT	WT	WT	WT	WT	WT	WT	WT	WT	WT	WT	WT	WT	WT
<i>cr-bnaap36-L3-1</i>	T <sub>1</sub>	WT	WT	WT	Homo (id)	WT	WT	WT	Homo (id)	WT	WT	Homo (id)	Homo (id)	WT	WT	WT	Homo (id)
<i>cr-bnaap36-L3-2</i>	T <sub>1</sub>	WT	WT	WT	Homo (id)	WT	WT	WT	Homo (id)	WT	WT	Homo (id)	Homo (id)	WT	WT	WT	Homo (id)
<i>cr-bnaap36-L3-3</i>	T <sub>1</sub>	WT	WT	WT	Homo (id)	WT	WT	WT	Homo (id)	WT	WT	Homo (id)	Homo (id)	WT	WT	WT	Homo (id)
<i>cr-bnaap36-L3-4</i>	T <sub>1</sub>	WT	WT	WT	Homo (id)	WT	WT	WT	Homo (id)	WT	WT	Homo (id)	Homo (id)	WT	WT	WT	Homo (id)
<i>cr-bnaap36-L3-5</i>	T <sub>1</sub>	WT	WT	WT	Homo (id)	WT	WT	WT	Homo (id)	WT	WT	Homo (id)	Homo (id)	WT	WT	WT	Homo (id)
<i>cr-bnaap36-L6</i>	T <sub>0</sub>	WT	WT	WT	Homo (id)	WT	WT	WT	Homo (id)	WT	WT	Homo (id)	Homo (id)	WT	WT	WT	Homo (i)
<i>cr-bnaap36-L6-1</i>	T <sub>1</sub>	WT	WT	WT	Homo (id)	WT	WT	WT	Homo (i)	WT	WT	Homo (i)	Homo (i)	WT	WT	WT	Homo (i)
<i>cr-bnaap36-L6-2</i>	T <sub>1</sub>	WT	WT	WT	Homo (i)	WT	WT	WT	Homo (i)	WT	WT	Homo (i)	Homo (i)	WT	WT	WT	Homo (i)
<i>cr-bnaap36-L6-3</i>	T <sub>1</sub>	WT	WT	WT	Homo (i)	WT	WT	WT	Homo (i)	WT	WT	Homo (i)	Homo (i)	WT	WT	WT	Homo (i)
<i>cr-bnaap36-L6-4</i>	T <sub>1</sub>	WT	WT	WT	Homo (i)	WT	WT	WT	Homo (i)	WT	WT	Homo (i)	Homo (i)	WT	WT	WT	Homo (i)

**Table 1** (continued)

<i>cr-bnaap36-L6-3</i>	T <sub>1</sub>	WT	WT	WT	WT	WT	WT	WT	Homo (i)	WT	WT	WT	WT	WT	Homo (i)
<i>cr-bnaap36-L6-4</i>	T <sub>1</sub>	WT	WT	WT	WT	WT	WT	WT	Homo (i)	WT	WT	WT	WT	WT	Homo (i)
<i>cr-bnaap36-L6-5</i>	T <sub>1</sub>	WT	WT	WT	WT	WT	WT	WT	Homo (i)	WT	WT	WT	WT	WT	Homo (i)
<i>cr-bnaap36-L7</i>	T <sub>0</sub>	WT	WT	WT	WT	WT	WT	WT	Hetero	WT	WT	WT	WT	WT	Hetero
<i>cr-bnaap36-L8</i>	T <sub>0</sub>	WT	WT	WT	WT	WT	WT	WT	WT	WT	WT	WT	WT	WT	WT
<i>cr-bnaap36-L9</i>	T <sub>0</sub>	WT	WT	WT	WT	WT	WT	WT	WT	WT	WT	WT	WT	WT	WT
<i>cr-bnaap36-L10</i>	T <sub>0</sub>	WT	WT	WT	WT	WT	WT	WT	Homo (i)	WT	WT	WT	WT	WT	Homo (d)
<i>cr-bnaap36-L11</i>	T <sub>0</sub>	WT	WT	WT	WT	WT	WT	WT	Hetero	WT	WT	WT	WT	WT	Hetero
<i>cr-bnaap36-L12</i>	T <sub>0</sub>	WT	WT	WT	WT	WT	WT	WT	Hetero	WT	WT	WT	WT	WT	Hetero

Hetero, heterozygous; Homo, homozygous; wt, no mutations were identified; #d, # of bp deleted from a target site; #i, # of bp inserted at target site; #s, # of bp substitute at target site

pollination of *cr-bnaap36* and *cr-bnaap39* stigma. After 24 h, approximately 34% and 36% of the WT PTs did not directly enter the micropyles (Fig. 5D). Therefore, micropylar guidance is impaired in the pollen tube of *cr-bnaap36* and *cr-bnaap39*. We speculate that the reduction in seed-set in *BnaAP36* and *BnaAP39* knockout mutants might be due to the failure of recognition between PTs and ovules.

## Discussion

The communication between female tissues and growing PTs is required for successful the double fertilization. Many components are involved in the regulation of micropyle-guided PTs growth (Müller et al. 2016). Here, we identified two aspartate proteases *BnaAP36s* and *BnaAP39s* in *B. napus*. Loss of function of *BnaAP36s* and *BnaAP39s* resulted in lower seed-set by mediating micropyle-guided PTs growth, indicating that the aspartate proteases play an important role in this process.

Aspartate proteases are hydrolytic enzymes that play an important role in plant reproduction (Ge et al. 2005). For example, rice aspartate proteases OsAP25, OsAP37 and OsAP65 are essential for tapetum degradation and pollen tube formation during pollen grain development (Huang et al. 2013). Further studies confirm that ETERNAL TAPE-TUM 1 (EAT1) promotes programmed cell death (PCD) of the tapetum by regulating the expression of *OsAP25* and *OsAP37* (Huang et al. 2013; Niu et al. 2013). We showed that anther-expressed *BnaAP36s* and *BnaAP39s* functioned as micropyle guides for PTs growth, while *BnaAP39* was also essential for maintaining the survival of mature pollen grains (Fig. 4A and B). Similar to *BnaAP36s* and *BnaAP39s*, the Arabidopsis AP36 and AP39 (A36 and A39) are involved in PTs micropyle guidance (Gao et al. 2017b). These results indicate that the conserved function of AP36 and AP39 in Arabidopsis and *B. napus*. Egg cell-specific APs, ECS1 and ECS2, have been shown to participate in micropyle-directed PT growth by degrading LURE (Yu et al. 2021). The PTs could be germinated on the papilla cells of the *BnaAP36* and *BnaAP39* knockout lines and grown in style (Fig. 5A). Meanwhile, abnormal micropylar-guided PTs growth was observed in *BnaAP36s* and *BnaAP39s* mutants (Fig. 5D), implying that the reduction the seed-set in *cr-bnaap36* and



**Table 2** Genotypic analysis of *BnaAP39s* mutants in T<sub>0</sub> and T<sub>1</sub> generations. (The red labeled ID indicated the two individual lines in this study)

Plant ID	Generation	genotype at targets of <i>BnaA06.AP39</i>		genotype at targets of <i>BnaC03.AP39</i>	
		sgRNA5	sgRNA6	sgRNA5	sgRNA6
<i>cr-bnaap39-L1</i>	T <sub>0</sub>	WT	Hetero	WT	Hetero
<i>cr-bnaap39-L2</i>	T <sub>0</sub>	WT	WT	WT	Hetero
<i>cr-bnaap39-L3</i>	T <sub>0</sub>	Hetero	WT	Hetero	Hetero
<i>cr-bnaap39-L4</i>	T <sub>0</sub>	Hetero	Hetero	Hetero	Hetero
<i>cr-bnaap39-L4-1</i>	T <sub>1</sub>	Hetero	Homo (i)	Hetero	Homo (i)
<i>cr-bnaap39-L4-2</i>	T <sub>1</sub>	Hetero	Homo (i)	Hetero	Homo (i)
<i>cr-bnaap39-L4-3</i>	T <sub>1</sub>	Hetero	Homo (i)	Hetero	Homo (i)
<i>cr-bnaap39-L4-4</i>	T <sub>1</sub>	Hetero	Homo (i)	Hetero	Homo (i)
<i>cr-bnaap39-L4-5</i>	T <sub>1</sub>	Hetero	Homo (i)	Hetero	Homo (i)
<i>cr-bnaap39-L5</i>	T <sub>0</sub>	WT	WT	Hetero	Hetero
<i>cr-bnaap39-L6</i>	T <sub>0</sub>	Hetero	Hetero	Hetero	Hetero
<i>cr-bnaap39-L7</i>	T <sub>0</sub>	Hetero	Hetero	Hetero	Hetero
<i>cr-bnaap39-L7-1</i>	T <sub>1</sub>	Hetero	Homo (i)	Hetero	Hetero
<i>cr-bnaap39-L7-2</i>	T <sub>1</sub>	WT	WT	WT	Hetero
<i>cr-bnaap39-L7-3</i>	T <sub>1</sub>	Hetero	Hetero	Hetero	Hetero
<i>cr-bnaap39-L7-4</i>	T <sub>1</sub>	Hetero	Hetero	Hetero	Hetero
<i>cr-bnaap39-L7-5</i>	T <sub>1</sub>	Hetero	WT	Hetero	Hetero
<i>cr-bnaap39-L8</i>	T <sub>0</sub>	Hetero	Hetero	Hetero	Hetero
<i>cr-bnaap39-L8-1</i>	T <sub>1</sub>	WT	WT	WT	Hetero
<i>cr-bnaap39-L8-2</i>	T <sub>1</sub>	WT	WT	WT	WT
<i>cr-bnaap39-L8-3</i>	T <sub>1</sub>	Hetero	Hetero	Hetero	Hetero
<i>cr-bnaap39-L8-4</i>	T <sub>1</sub>	Hetero	WT	Hetero	Hetero
<i>cr-bnaap39-L8-5</i>	T <sub>1</sub>	WT	WT	WT	Hetero
<i>cr-bnaap39-L9</i>	T <sub>0</sub>	Hetero	WT	Hetero	Hetero
<i>cr-bnaap39-L9-1</i>	T <sub>1</sub>	Homo (id)	WT	Homo (id)	Homo (i)
<i>cr-bnaap39-L9-2</i>	T <sub>1</sub>	Homo (id)	WT	Homo (id)	Homo (i)
<i>cr-bnaap39-L9-3</i>	T <sub>1</sub>	Homo (id)	WT	Homo (id)	Homo (i)
<i>cr-bnaap39-L9-4</i>	T <sub>1</sub>	Homo (id)	WT	Homo (id)	Homo (i)
<i>cr-bnaap39-L9-5</i>	T <sub>1</sub>	Homo (id)	WT	Homo (id)	Homo (i)

Hetero, heterozygous;  
Homo, homozygous; wt, no  
mutations were identified;  
#d, #of bp deleted from  
a target site; #i, # of bp  
inserted at target site; #s,  
#of bp substitute at target  
site

*cr-bnaap39* could be due to the failure of recognition between pollen tubes and ovules. One possibility is that BnaAP36 and BnaAP39 may regulate the growth of micropylar-guided PTs through degradation of the proteins that block pollen guidance.

There is complex signal regulation between pollen tube and ovule recognition. For instance, the Arabidopsis synergid cells secrete the pollen tube attraction signal *LURE1*, which is recognized by the pollen-specific receptor-like kinases, LIP1 and LIP2 (Lost in Pollen Tube Guidance 1 and 2), regulating pollen tube growth and guidance (Takeuchi and Higashiyama 2016; Liu et al. 2013). We identified

BnaAP36s and BnaAP39s as GPI-modified aspartate proteases (Fig. 1 and Fig. 5). Approximately 35% the pollen tubes lose the ability to direct growth towards micropores in *BnaAP36s* and *BnaAP39s* mutants' style (Fig. 5E). In loss-of-function mutants of other GPI-anchored proteins, A36, A39, and COBL10, PTs also fail to target the ovule (Gao et al. 2017a). GPI-anchored proteins are localized in lipid rafts, which serve as the platforms for protein trafficking and cell signaling transduction (Varma and Mayor 1998). We speculate that BnaAP36s and BnaAP39s might have some relationship with LIP1/ LIP2- LURE1 cassette, which needs to be investigated in the future.

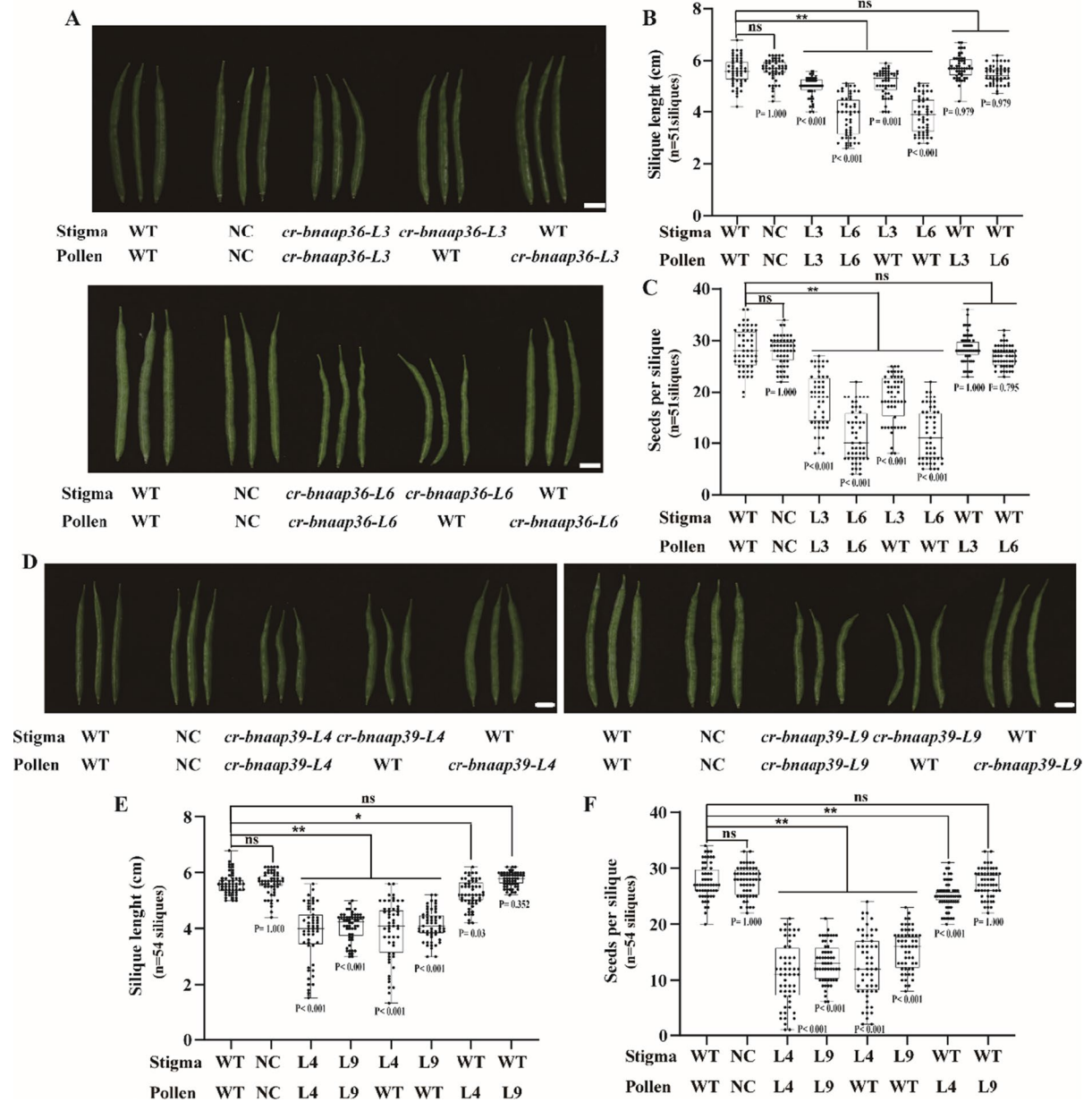


**Fig. 3** Seed-set was reduced in *cr-bnaap36* and *cr-bnaap39* mutants. **(A)** The images showed the siliques of *cr-bnaap36* sextuple mutants after self-cross and reciprocal crosses with WT. Scale bars: 1 cm. **(B)** and **(C)** The bar graph showed the silique length **(B)** and seed-set **(C)** in **(A)**. **(D)** The images showed the siliques of *cr-bnaap39* double mutants after self-cross and reciprocal crosses with WT. Scale bars: 1cm. **(E)** and **(F)** The bar graph showed the silique length **(B)** and seed-set **(C)** in **(D)**. In **(B)**, **(C)**, **(E)**, and **(F)**, the experiment was repeated three times independently. In each replicate, five individual plants of each line were randomly selected. In each

individual plant, at least ten stigmas were randomly pollinated. After pollination, 50 siliques from each line were measured. The seed-set was calculated as the number of seeds per each silique. In **(B)**, **(C)**, **(E)**, and **(F)**, all statistical analyses were calculated in SPSS version 19.0. Error bars were expressed as mean  $\pm$  SE. P values were obtained by one-way ANOVA with multiple comparisons.  $P > 0.05$  (ns),  $P < 0.05$  (\*),  $P < 0.01$  (\*\*). WT: Wild type; NC: transgenic negative plants; L3 and L6: two independent *cr-bnaap36* lines; L4 and L9: two independent *cr-bnaap39* lines

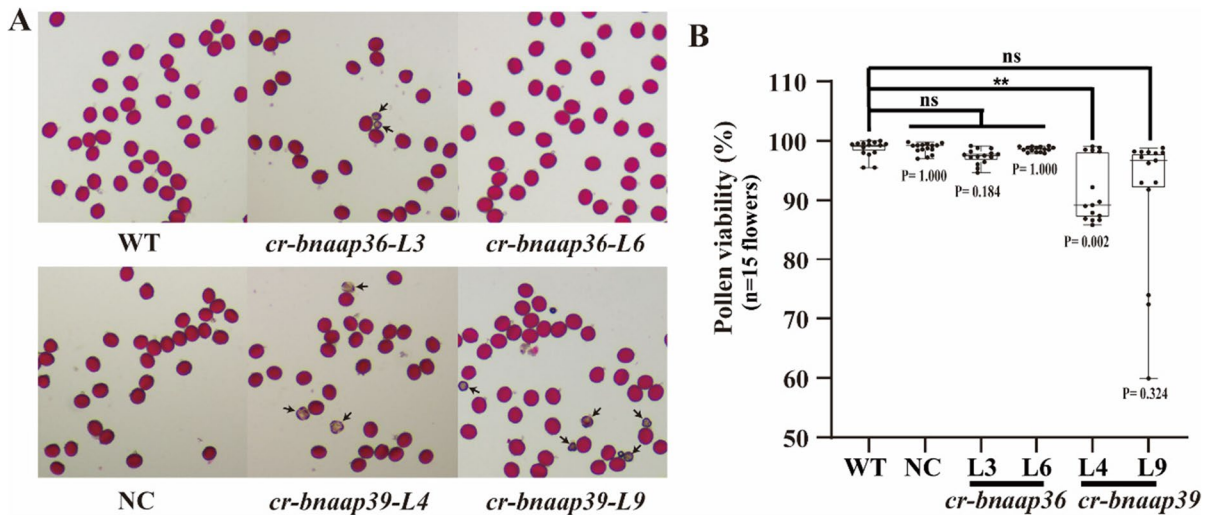


**Fig. 4** The viability of mature pollen grains of *cr-bnaap36* and *cr-bnaap39* mutants. **(A)** The viability of mature pollen grains of different materials was observed by Alexander staining. **(B)** Quantification of pollen activities from different materials. I The experiment was repeated three times independently. In each replicate, five individual plants of each line were selected, and three flowers from each individual plant were randomly selected. More than 1000 pollen grains were counted

*Brassica napus* (AACC) is an important allopolyploid crop derived from interspecific crosses between *Brassica rapa* and *Brassica oleracea* (Chalhoub et al. 2014; Ahmad et al. 2023). The Arabidopsis homologous genes in *B. napus* are multiple copies with high sequence similarity. Six and two homologs of *BnaAP36* and *BnaAP39*, respectively, were identified in the *B. napus* genome with conserved protein domains (Fig. S2 and S3). Although the expression levels of *BnaAP36* and *BnaAP39* homologs were slightly different, these homologs showed the similar tissue expression patterns (Fig. 1C–D and S4), indicating *BnaAP36s* and *BnaAP39s* might function redundantly in *B. napus*. Indeed, the sextuple and double mutants of *BnaAP36* and *BnaAP39* showed reduced seed-set, and PTs failed to grow towards the micropyle (Fig. 5); whereas the single mutants of *BnaAP36* and *BnaAP39* didn't show any defects in micropylar guidance, suggesting the functional redundancy among different homologs. Notably, the reduction in seed-set of *BnaAP36* and *BnaAP39* mutants was more severe than that of Arabidopsis *A36* and *A39* single gene mutants (Fig. 5) (Gao et al. 2017b), and the pollen abortion occurred in the

for statistical analysis. In **(B)**, the statistical analyses were calculated in SPSS version 19.0. Error bars were expressed as mean  $\pm$  SE. P values were obtained by one-way ANOVA with multiple comparisons.  $P > 0.05$  (ns),  $P < 0.05$  (\*),  $P < 0.01$  (\*\*). WT: Wild type; NC: transgenic negative plants; L3 and L6: two independent *cr-bnaap36* lines; L4 and L9: two independent *cr-bnaap39* lines

*BnaAP39* mutants, but not in the *BnaAP36* mutants (Fig. 4), suggesting that the functional differentiation of *BnaAP36s* and *BnaAP39s* might be affected by polyploidization process.

## Material and Methods

### Plant materials and growth condition

All *BnaAP36s* and *BnaAP39s* mutants and wild-type (Westar, self-compatible) seeds were soaked in water for 7 days and then placed in soil and grown in the transgenic plant field at Huazhong Agricultural University. *Arabidopsis thaliana* transgenic lines, and tobacco (*Nicotiana benthamiana*) were grown in the greenhouse under a light intensity of  $100 \mu\text{mol m}^{-2}\text{s}^{-1}$  with a 16/8 h light/dark photoperiod at  $22^\circ\text{C}$ .

### Plasmid construction

The genes were amplified from *B. napus* DNA library by PCR using gene-specific primers. For the GUS staining assay, the ~2kb promoters of *BnaC08.AP36*

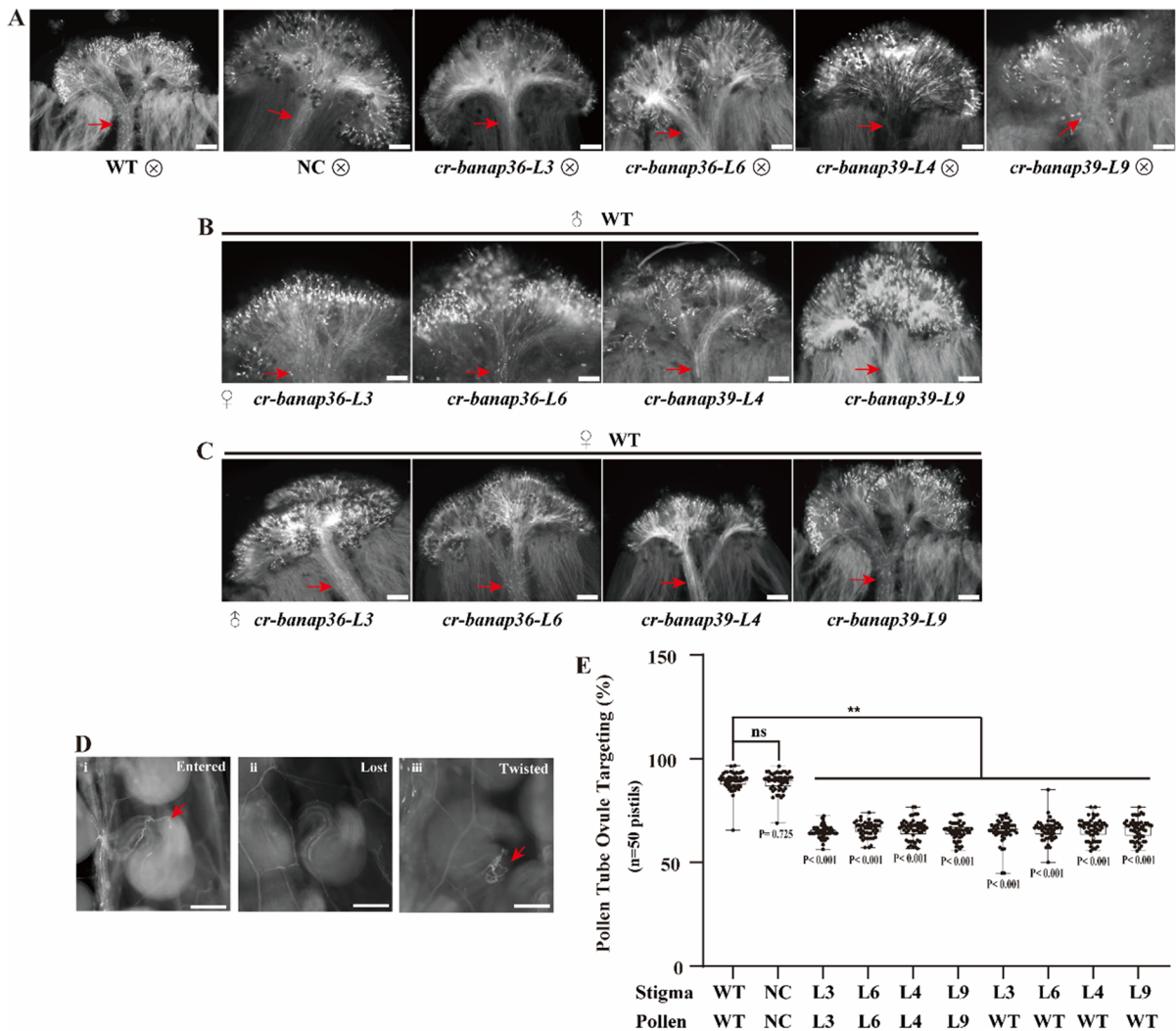


**Fig. 5** Abnormal pollen tube guidance in *BnaAP36* and *BnaAP39* mutants. **(A)** The images showed the pollen tube growth of *cr-bnaap36* sextuple and *cr-bnaap39* double mutants after self-crossing by aniline blue assay. Red arrows indicated the pollen tube bundles. Scale bars: 100  $\mu$ m. **(B)** The images showed the pollen tube growth of *cr-bnaap36* sextuple and *cr-bnaap39* double mutants after reciprocal crosses with WT by aniline blue assay. Red arrows indicated the pollen tube bundles. Scale bars: 100  $\mu$ m. **(C)** The images showed the defective navigation of *cr-bnaap36* sextuple mutant pollen tubes. Pollen tubes were stained with aniline blue and visualized by fluorescence microscopy. i: WT self-pollination. WT pollen tubes enter the micropyle directly. ii and iii: *cr-bnaap36-L3* self-pollination. The pollen tubes missed the micropyle (i) or twisted

around the ovule surface (ii). Bar = 100  $\mu$ m. Arrows indicate the pollen tubes. **(D)** The bar graph showed the statistical analysis of the percentage of pollen tubes targeting the ovule. The experiment was repeated three times independently. In each replicate, five individual plants from each line were selected, and ten stigmas of each plant were randomly pollinated. After pollination, 50 pistils from each line were stained and the number of ovule-directed pollen tubes was calculated for each pistil. In **(E)**, the statistical analyses were calculated in SPSS version 19.0. Error bars were expressed as mean  $\pm$  SE. P values were obtained by one-way ANOVA with multiple comparison.  $P > 0.05$  (ns),  $P < 0.05$  (\*),  $P < 0.01$  (\*\*). WT: Wild type; NC: transgenic negative plants; L3 and L6: two independent *cr-bnaap36* lines; L4 and L9: two independent *cr-bnaap39* lines



and *BnaA06.AP39* were amplified by PCR and cloned into the vector pCAMBIA2300::*GUS*, respectively. For the subcellular localization assay, the CDS of *BnaC08.AP36* and *BnaA06.AP39* were amplified by PCR and then cloned into pRII101-GFP vector. To generate *BnaAP36s* and *BnaAP39s* mutants, the *GENE-sgRNA* plant expression vectors were constructed as previously described with minor modifications (Xing et al. 2014). Briefly, four and two sgRNAs were designed to target the homologues of the *BnaAP36* and *BnaAP39* exons by CRISPR-P (<http://cbi.hzau.edu.cn/cgi-bin/CRISPR>), respectively (Lei et al. 2014). The sgRNAs cassettes were amplified by PCR using *pCBC-DT<sub>1</sub>T<sub>2</sub>* as template, and the PCR fragments were then inserted into *pKSE401G* by Golden Gate Assembly (Gao et al. 2013). All primers were listed in Table S4.

#### Plant transformation and genotyping

The procedure of *Agrobacterium*-mediated transformation of *B. napus* (Westar, self-compatible) was performed as previously described (Dai et al. 2020). To genotype the CRISPR/Cas9-mediated mutation, the CTAB method was used to extract the genomic DNA (Molecular Cloning 4<sup>th</sup> edition). The targeted mutations were determined in transgenic plants using the Hi-TOM platform (Liu et al. 2019). Target-specific and barcoding PCR, two rounds of PCR, were performed to amplify the genomic region containing the specific targets of independent samples, and the resulting PCR products were mixed in equal amounts and purified for next-generation sequencing (the Illumina HiSeq platform at Novogene Bioinformatics Institute, Beijing, China). The resulting sequencing data were then decoded using a dedicated online tool to track mutations at the target sites (<http://www.hi-tom.net/hi-tom/>). The target-specific primer sets are listed in Table S5.

#### RNA isolation and reverse-transcription quantitative PCR (RT-qPCR)

The *B. napus* root, stem, leaf, flower bud (2 mm 4 mm and 6 mm), seed, silique, sepal, petal, stigma, ovary, anther, and filament were collected and immediately frozen in liquid nitrogen. Total RNA was extracted using an RNAPrep pure plant kit (TIANGEN Cat. #DP441) according to the manufacturer's

instructions. The cDNA was synthesized using a Transcript RT kit (TaKaRa, Japan, Cat. #RR047A). For RT-qPCR, a total volume of 10  $\mu$ L of reaction mixtures was used, containing 5  $\mu$ L of 2 $\times$ SYBR Green Master Mix (BioRad, USA), 4.6  $\mu$ L of 100 $\times$  diluted cDNA, 0.2  $\mu$ L of each primer. Amplification was performed using a CFX384 Real-Time System (TOYOBO, JAPAN). The amplification program was carried out as previously describe (Wu et al. 2020). *BnaActin7* was used as an internal reference. The expression level of each gene was calculated using the  $2^{-\Delta\text{CT}}$  method. All analyses were repeated at least three times. Primers used for RT-qPCR were listed in Supplemental Table S6.

#### Measurement of seeds per silique

The stigmas were emasculated one day before anthesis to avoid pollen contamination. The emasculated stigmas were then sufficiently pollinated with WT's or mutant's pollen. After pollination, the stigmas were covered with paper bags and kept for 10 days. The bags were then removed, and mature siliques were opened to calculate the number of seeds and silique length. The experiment was repeated three times independently. In each replicate, five individual plants of each line were randomly selected. In each individual plant, at least ten stigmas were randomly pollinated. After pollination, 50 siliques from each line were measured. The seed-set was calculated as the number of seeds per each silique.

#### Pollen viability assay

Pollen grains from fully opened flowers were used pollen viability analysis. Pollen viability was determined as the percentage of stained pollen grains in Alexander. The experiment was repeated three times independently. In each replicate, five individual plants of each line were selected, and three flowers from each individual plant were randomly selected. More than 1000 pollen grains were counted for statistical analysis.

#### Aniline blue assay

The aniline blue staining assay was performed according to the established procedure, with minor modifications (Sankaranarayanan et al. 2015). The anther was removed the day before anthesis. The emasculated stigmas were



pollinated with the corresponding pollen on the day of flowering. After 24 h, the pollinated pistils were placed in fixative buffer (3:1 ethanol, glacial acetic acid) for 2 h, and then the samples were incubated in 1 M NaOH at 65 °C water for 1 h. The pistils were then washed three times with distilled water and stained with the basic aniline blue stain (0.1% aniline blue staining in 0.1 M K<sub>3</sub>PO<sub>4</sub>) for 3 h. The stained pistils were placed on a glass slide in distilled water to detect the pollen germination and pollen tube growth using the blue channel (UV 340–380 nm) of a fluorescence microscope (SP8; Leica, Wetzlar, Germany). The experiment was repeated three times independently. In each replicate, five individual plants from each line were selected, and ten stigmas of each plant were randomly pollinated. After pollination, 50 pistils from each line were stained and the number of ovule-directed pollen tubes was calculated for each pistil.

#### Phylogeny tree and sequence alignment analysis

Amino acid sequences of BnaAP36 and BnaAP39 homologs were downloaded from BnIR (<http://yanglab.hzau.edu.cn/BnIR>) and Brassicaceae Database (<http://brassicadb.cn>). The MEGA software (version 7.0) was used for sequence alignment and clustering analysis by the nearest neighbor method with 1000 bootstrap replicates. The visualization of the sequence alignment results was performed using GeneDoc (version 2.7). The GPI-anchor sequence was predicted by big-PI Pre-dictor ([http://mendel.imp.ac.at/gpi/gpi\\_server.html](http://mendel.imp.ac.at/gpi/gpi_server.html)) (Eisenhaber et al. 1998).

#### Subcellular localization assay

The protein subcellular localization analysis in *N. benthamiana* was performed as previously described (Yang et al. 2021). Briefly, in *N. benthamiana*, *Agrobacterium tumefaciens* (strain GV3101) cells containing the desired constructs were co-infiltrated into 4- to 5-week-old *N. benthamiana* leaves with infiltration buffer (50 mM MES, pH=5.6, 2 mM Na<sub>3</sub>PO<sub>4</sub> and 1 mM acetosyringone). The final bacteria concentrations were adjusted to an OD<sub>600</sub> = 0.6 for each construct. Infected leaves were analyzed at 48 h after infiltration. GFP fluorescence (Excitation /Emission wavelength: 488 nm / 509 nm), and RFP fluorescence (Excitation / Emission wavelength: 559 nm / 583 nm) were observed under a fluorescence microscope (SPX8, Leica).

#### GUS staining assay

Two *GUS* reporter constructs (*pBnaC08.AP36::GUS* and *pBnaA06.AP39::GUS*) were generated and individually transformed into *Arabidopsis* by the floral dipping method (Clough and Bent 1998). Positive transgenic lines were obtained in the T<sub>1</sub> generation and GUS staining assay was performed. For the GUS staining assay, the tissues were immersed in X-Gluc solution (Coolaber, SL7160), and incubated at 37 °C overnight. The stained tissues were then photographed under a microscope as previously described (Liu et al. 2020). The experiment was replicated three times independently. In each replicate, five individual plants from each line were selected.

#### Statistical analyses

Statistical analysis was conducted using SPSS version 19.0 (IBM; <https://www.ibm.com>). Error bars were expressed as mean ± SE. P values were obtained by one-way ANOVA with multiple comparisons. *P* > 0.05 (ns), *P* < 0.05 (\*), *P* < 0.01 (\*\*).

**Acknowledgements** The authors extend their appreciation to the support from National Key Laboratory of Crop Genetic Improvement and Hubei Hongshan Laboratory, Huazhong Agricultural University.

**Funding Support** This study was supported by the NSFC (No. 32172070) to Chaozhi Ma, and NSFC (No. 32072105) to Cheng Dai.

**Author contributions** C.D., and L.W. designed the research. L.W., and X.L. performed the experiments. B.Y., T.F., and C.M. provided lab support. S.D., and L.W. analyzed the data. C.D., and L.W. wrote the manuscript. All authors read and approved the manuscript.

**Data availability** Not applicable.

**Ethics declarations**

**Ethics approval** All authors approved the submission.

**Consent to participate** N/A

**Consent for publication** Yes.

**Conflict of interest** The authors declare no conflicts of interest.

## References

- Ahmad A, Li W, Zhang H, Wang H, Wang P, Jiao Y, Zhao C, Yang G, Hong D (2023) Linkage and association mapping of ovule number per ovary (ON) in oilseed rape (*Brassica napus* L.). *Mol Breed* 43(2):1–16. <https://doi.org/10.1007/s11032-023-01355-7>
- Berger F, Hamamura Y, Ingouff M, Higashiyama T (2008) Double fertilization - caught in the act. *Trends Plant Sci* 13(8):437–443. <https://doi.org/10.1016/j.tplants.2008.05.011>
- Chalhoub B, Denoeud F, Liu S, Parkin IA, Tang H, Wang X, Chiquet J, Belcram H, Tong C, Samans B, Corréa M, Da Silva C, Just J, Falentin C, Koh CS, Le Clainche I, Bernard M, Bento P, Noel B et al (2014) Plant genetics. Early allopolyploid evolution in the post-Neolithic *Brassica napus* oilseed genome. *Science* 345(6199):950–953. <https://doi.org/10.1126/science.1253435>
- Chen D, Jin Q, Pan J, Liu Y, Tang Y, E Y, Xu L, Yang T, Qiu J, Chen X, Wang J, Gong D, Ge X, Li Z, Cui C (2023) Fine mapping of genes controlling pigment accumulation in oilseed rape (*Brassica napus* L.). *Mol Breed* 43 (3):19. <https://doi.org/10.1007/s11032-023-01365-5>
- Clough SJ, Bent AF (1998) Floral dip: a simplified method for *Agrobacterium*-mediated transformation of *Arabidopsis thaliana*. *Plant J* 16(6):735–743. <https://doi.org/10.1046/j.1365-3113x.1998.00343.x>
- Dai C, Li Y, Li L, Du Z, Lin S, Tian X, Li S, Yang B, Yao W, Wang J, Guo L, Lu S (2020) An efficient *Agrobacterium*-mediated transformation method using hypocotyl as explants for *Brassica napus*. *Mol Breed* 40(10). <https://doi.org/10.1007/s11032-020-01174-0>
- Dresselhaus T, Sprunck S, Wessel GM (2016) Fertilization Mechanisms in Flowering Plants. *Curr Biol* 26(3):R125–R139. <https://doi.org/10.1016/j.cub.2015.12.032>
- Eisenhaber B, Bork P, Eisenhaber F (1998) Sequence properties of GPI-anchored proteins near the omega-site: constraints for the polypeptide binding site of the putative transamidase. *Protein Eng* 11(12):1155–1161. <https://doi.org/10.1093/protein/11.12.1155>
- Escobar-Restrepo JM, Huck N, Kessler S, Gagliardini V, Gheyselinck J, Yang WC, Grossniklaus U (2007) The FERONIA receptor-like kinase mediates male-female interactions during pollen tube reception. *Science* 317(5838):656–660. <https://doi.org/10.1126/science.1143562>
- Galindo-Trigo S, Blanco-Touriñán N, DeFalco TA, Wells ES, Gray JE, Zipfel C, Smith LM (2020) CrRLKIL receptor-like kinases HERK1 and ANJEA are female determinants of pollen tube reception. *EMBO Rep* 21(2):e48466. <https://doi.org/10.15252/embr.201948466>
- Gao H, Li R, Guo Y (2017a) *Arabidopsis* aspartic proteases A36 and A39 play roles in plant reproduction. *Plant Signal Behav* 12(4):e1304343. <https://doi.org/10.1080/15592324.2017.1304343>
- Gao H, Zhang Y, Wang W, Zhao K, Liu C, Bai L, Li R, Guo Y (2017b) Two Membrane-Anchored Aspartic Proteases Contribute to Pollen and Ovule Development. *Plant Physiol* 173(1):219–239. <https://doi.org/10.1104/pp.16.01719>
- Gao X, Yan P, Shen W, Li X, Zhou P, Li Y (2013) Modular construction of plasmids by parallel assembly of linear vector components. *Anal Biochem* 437(2):172–177. <https://doi.org/10.1016/j.ab.2013.02.028>
- Ge X, Dietrich C, Matsuno M, Li G, Berg H, Xia Y (2005) An *Arabidopsis* aspartic protease functions as an anti-cell-death component in reproduction and embryogenesis. *EMBO Rep* 6(3):282–288. <https://doi.org/10.1038/sj.embor.7400357>
- Higashiyama T, Takeuchi H (2015) The mechanism and key molecules involved in pollen tube guidance. *Annu Rev Plant Biol* 66:393–413. <https://doi.org/10.1146/annurev-arplant-043014-115635>
- Hu J, Chen B, Zhao J, Zhang F, Xie T, Xu K, Gao G, Yan G, Li H, Li L, Ji G, An H, Li H, Huang Q, Zhang M, Wu J, Song W, Zhang X, Luo Y et al (2022) Genomic selection and genetic architecture of agronomic traits during modern rapeseed breeding. *Nat Genet* 54(5):694–704. <https://doi.org/10.1038/s41588-022-01055-6>
- Huang C, Liang X, Dai C, Wen J, Yi B, Tu J, Shen J, Fu T, Ma C (2022) Genome wide analysis of *BnAPs* gene family in *Brassica napus*. *Acta Agronomica Sinica (China)* 48(3):597–607. <https://doi.org/10.3724/SP.J.1006.2022.14023>
- Huang J, Zhao X, Cheng K, Jiang Y, Ouyang Y, Xu C, Li X, Xiao J, Zhang Q (2013) OsAP65, a rice aspartic protease, is essential for male fertility and plays a role in pollen germination and pollen tube growth. *J Exp Bot* 64(11):3351–3360. <https://doi.org/10.1093/jxb/ert173>
- Kato Y, Yamamoto Y, Murakami S, Sato F (2005) Post-translational regulation of CND41 protease activity in senescent tobacco leaves. *Planta* 222(4):643–651. <https://doi.org/10.1007/s00425-005-0011-4>
- Lausser A, Dresselhaus T (2010) Sporophytic control of pollen tube growth and guidance in grasses. *Biochem Soc Trans* 38(2):631–634. <https://doi.org/10.1042/bst0380631>
- Lei Y, Lu L, Liu HY, Li S, Xing F, Chen LL (2014) CRISPR-P: a web tool for synthetic single-guide RNA design of CRISPR-system in plants. *Mol Plant* 7(9):1494–1496. <https://doi.org/10.1093/mp/ssu044>
- Liu D, Yu L, Wei L, Yu P, Wang J, Zhao H, Zhang Y, Zhang S, Yang Z, Chen G, Yao X, Yang Y, Zhou Y, Wang X, Lu S, Dai C, Yang QY, Guo L (2021) BnTIR: an online transcriptome platform for exploring RNA-seq libraries for oil crop *Brassica napus*. *Plant Biotechnol J* 19(10):1895–1897. <https://doi.org/10.1111/pbi.13665>
- Liu J, Zhong S, Guo X, Hao L, Wei X, Huang Q, Hou Y, Shi J, Wang C, Gu H, Qu LJ (2013) Membrane-bound RLCKs LIP1 and LIP2 are essential male factors controlling male-female attraction in *Arabidopsis*. *Curr Biol* 23(11):993–998. <https://doi.org/10.1016/j.cub.2013.04.043>
- Liu Q, Wang C, Jiao X, Zhang H, Song L, Li Y, Gao C, Wang K (2019) Hi-TOM: a platform for high-throughput tracking of mutations induced by CRISPR/Cas systems. *Sci China Life Sci* 62(1):1–7. <https://doi.org/10.1007/s11427-018-9402-9>
- Liu Y, Ye S, Yuan G, Ma X, Heng S, Yi B, Ma C, Shen J, Tu J, Fu T, Wen J (2020) Gene silencing of *BnaA09.ZEP* and *BnaC09.ZEP* confers orange color in *Brassica napus* flowers. *Plant J* 104 (4):932–949. <https://doi.org/10.1111/tpj.14970>

- Márton ML, Cordts S, Broadhvest J, Dresselhaus T (2005) Micropylar pollen tube guidance by egg apparatus 1 of maize. *Science* 307(5709):573–576. <https://doi.org/10.1126/science.1104954>
- Müller LM, Lindner H, Pires ND, Gagliardini V, Grossniklaus U (2016) A subunit of the oligosaccharyltransferase complex is required for interspecific gametophyte recognition in Arabidopsis. *Nat Commun* 7:10826. <https://doi.org/10.1038/ncomms10826>
- Niu N, Liang W, Yang X, Jin W, Wilson ZA, Hu J, Zhang D (2013) EAT1 promotes tapetal cell death by regulating aspartic proteases during male reproductive development in rice. *Nat Commun* 4:1445. <https://doi.org/10.1038/ncomms2396>
- Palanivelu R, Tsukamoto T (2012) Pathfinding in angiosperm reproduction: pollen tube guidance by pistils ensures successful double fertilization. *Wiley Interdiscip Rev Dev Biol* 1(1):96–113. <https://doi.org/10.1002/wdev.6>
- Prasad BD, Creissen G, Lamb C, Chattoo BB (2009) Overexpression of rice (*Oryza sativa* L.) OsCDR1 leads to constitutive activation of defense responses in rice and Arabidopsis. *Mol Plant-Microbe Interact* 22(12):1635–1644. <https://doi.org/10.1094/mpmi-22-12-1635>
- Sankaranarayanan S, Jamshed M, Samuel MA (2015) Degradation of glyoxalase I in *Brassica napus* stigma leads to self-incompatibility response. *Nat Plants* 1:15185. <https://doi.org/10.1038/nplants.2015.185>
- Shen W, Yao X, Ye T, Ma S, Liu X, Yin X, Wu Y (2018) Arabidopsis Aspartic Protease ASPG1 Affects Seed Dormancy, Seed Longevity and Seed Germination. *Plant Cell Physiol* 59(7):1415–1431. <https://doi.org/10.1093/pcp/pcy070>
- Simões I, Faro C (2004) Structure and function of plant aspartic proteinases. *Eur J Biochem* 271(11):2067–2075. <https://doi.org/10.1111/j.1432-1033.2004.04136.x>
- Soares A, Niedermaier S, Faro R, Loos A, Manadas B, Faro C, Huesgen PF, Cheung AY, Simões I (2019) An atypical aspartic protease modulates lateral root development in Arabidopsis thaliana. *J Exp Bot* 70(7):2157–2171. <https://doi.org/10.1093/jxb/erz059>
- Swanson R, Edlund AF, Preuss D (2004) Species specificity in pollen-pistil interactions. *Annu Rev Genet* 38:793–818. <https://doi.org/10.1146/annurev.genet.38.072902.092356>
- Takahashi K, Niwa H, Yokota N, Kubota K, Inoue H (2008) Widespread tissue expression of nepenthesin-like aspartic protease genes in Arabidopsis thaliana. *Plant Physiol Biochem* 46(7):724–729. <https://doi.org/10.1016/j.plaphy.2008.04.007>
- Takeuchi H, Higashiyama T (2016) Tip-localized receptors control pollen tube growth and LURE sensing in Arabidopsis. *Nature* 531(7593):245–248. <https://doi.org/10.1038/nature17413>
- Tang T, Yu X, Yang H, Gao Q, Ji H, Wang Y, Yan G, Peng Y, Luo H, Liu K, Li X, Ma C, Kang C, Dai C (2018) Development and Validation of an Effective CRISPR/Cas9 Vector for Efficiently Isolating Positive Transformants and Transgene-Free Mutants in a Wide Range of Plant Species. *Front Plant Sci* 9:1533. <https://doi.org/10.3389/fpls.2018.01533>
- Varma R, Mayor S (1998) GPI-anchored proteins are organized in submicron domains at the cell surface. *Nature* 394(6695):798–801. <https://doi.org/10.1038/29563>
- Wang T, Liang L, Xue Y, Jia PF, Chen W, Zhang MX, Wang YC, Li HJ, Yang WC (2016) A receptor heteromer mediates the male perception of female attractants in plants. *Nature* 531(7593):241–244. <https://doi.org/10.1038/nature16975>
- Weterings K, Russell SD (2004) Experimental analysis of the fertilization process. *Plant Cell* 16:S107–S118. <https://doi.org/10.1105/tpc.016873>
- Wu J, Yan G, Duan Z, Wang Z, Kang C, Guo L, Liu K, Tu J, Shen J, Yi B, Fu T, Li X, Ma C, Dai C (2020) Roles of the Brassica napus DELLA Protein BnaA6.RGA, in Modulating Drought Tolerance by Interacting With the ABA Signaling Component BnaA10.ABF2. *Front. Plant Sci* 11:577. <https://doi.org/10.3389/fpls.2020.00577>
- Xia Y, Suzuki H, Borevitz J, Blount J, Guo Z, Patel K, Dixon RA, Lamb C (2004) An extracellular aspartic protease functions in Arabidopsis disease resistance signaling. *EMBO J* 23(4):980–988. <https://doi.org/10.1038/sj.emboj.7600086>
- Xing HL, Dong L, Wang ZP, Zhang HY, Han CY, Liu B, Wang XC, Chen QJ (2014) A CRISPR/Cas9 toolkit for multiplex genome editing in plants. *BMC Plant Biol* 14:327. <https://doi.org/10.1186/s12870-014-0327-y>
- Yang B, Zhang K, Jin X, Yan J, Lu S, Shen Q, Guo L, Hong Y, Wang X, Guo L (2021) Acylation of non-specific phospholipase C4 determines its function in plant response to phosphate deficiency. *Plant J* 106(6):1647–1659. <https://doi.org/10.1111/tpj.15260>
- Yao X, Xiong W, Ye T, Wu Y (2012) Overexpression of the aspartic protease ASPG1 gene confers drought avoidance in Arabidopsis. *J Exp Bot* 63(7):2579–2593. <https://doi.org/10.1093/jxb/err433>
- Yu X, Zhang X, Zhao P, Peng X, Chen H, Bleckmann A, Bazhenova A, Shi C, Dresselhaus T, Sun MX (2021) Fertilized egg cells secrete endopeptidases to avoid polytubey. *Nature* 592(7854):433–437. <https://doi.org/10.1038/s41586-021-03387-5>
- Zhang T, Gao C, Yue Y, Liu Z, Ma C, Zhou G, Yang Y, Duan Z, Li B, Wen J, Yi B, Shen J, Tu J, Fu T (2017a) Time-Course Transcriptome Analysis of Compatible and Incompatible Pollen-Stigma Interactions in Brassica napus L. *Front Plant Sci* 8:682. <https://doi.org/10.3389/fpls.2017.00682>
- Zhang X, Liu W, Nagae TT, Takeuchi H, Zhang H, Han Z, Higashiyama T, Chai J (2017b) Structural basis for receptor recognition of pollen tube attraction peptides. *Nat Commun* 8(1):1331. <https://doi.org/10.1038/s41467-017-01323-8>
- Zhong S, Li L, Wang Z, Ge Z, Li Q, Bleckmann A, Wang J, Song Z, Shi Y, Liu T, Li L, Zhou H, Wang Y, Zhang L, Wu HM, Lai L, Gu H, Dong J, Cheung AY et al (2022) RALF peptide signaling controls the polytubey block in Arabidopsis. *Science* 375(6578):290–296. <https://doi.org/10.1126/science.abl4683>
- Zhong S, Qu LJ (2019) Peptide/receptor-like kinase-mediated signaling involved in male-female interactions. *Curr Opin Plant Biol* 51:7–14. <https://doi.org/10.1016/j.pbi.2019.03.004>

Zhong S, Liu M, Wang Z, Huang Q, Hou S, Xu YC, Ge Z, Song Z, Huang J, Qiu X, Shi Y, Xiao J, Liu P, Guo YL, Dong J, Dresselhaus T, Gu H, Qu LJ (2019) Cysteine-rich peptides promote interspecific genetic isolation in *Arabidopsis*. *Science* 364(6443). <https://doi.org/10.1126/science.aau9564>

**Publisher's note** Springer Nature remains neutral with regard to jurisdictional claims in published maps and institutional affiliations.

Springer Nature or its licensor (e.g. a society or other partner) holds exclusive rights to this article under a publishing agreement with the author(s) or other rightsholder(s); author self-archiving of the accepted manuscript version of this article is solely governed by the terms of such publishing agreement and applicable law.